Cystic Fibrosis Transmembrane Conductance Regulator: Solution Structures of Peptides Based on the Phe508 Region, the Most Common Site of Disease-Causing ΔF508 Mutation[†,‡]

Michael A. Massiah, Young-Hee Ko,[§] Peter L. Pedersen, and Albert S. Mildvan*

Department of Biological Chemistry, Johns Hopkins University, School of Medicine, 725 North Wolfe Street, Baltimore, Maryland 21205-2185

Received February 15, 1999; Revised Manuscript Received April 12, 1999

ABSTRACT: Most cases of cystic fibrosis (CF), a common inherited disease of epithelial cell origin, are caused by the deletion of Phe508 located in the first nucleotide-binding domain (NBF1) of the protein called CFTR (cystic fibrosis transmembrane conductance regulator). To gain greater insight into the structure within the Phe508 region of the wild-type protein and the change in structure that occurs when this residue is deleted, we conducted nuclear magnetic resonance (NMR) studies on representative synthetic 26 and 25 amino acid peptide segments. 2D ^{1}H NMR studies at 600 MHz of the 26-residue peptide consisting of Met498 to Ala523 in 10% DMSO, pH 4.0, at 25 °C show a continuous but labile helix from Gly500 to Lys522, based on both NH−NH$_{(i,i+1)}$ and αH−NH$_{(i,i+1)}$ NOEs. Phe508 within this helix shows only short-range (i, $\leq i + 2$) NOEs. The corresponding 25-residue peptide lacking Phe508 also forms a labile helix from Gly500 to Lys522. However, the relative intensities of the NH−NH$_{(i,i+1)}$/αH−NH$_{(i,i+1)}$ NOEs, fewer intermediate-range NOEs, and downfield αH and NH chemical shifts indicate a lower helical propensity of the 25-mer between residues 505 and 517, surrounding the missing residue, Phe508. 2D ^{1}H NMR studies of both peptides in saturating (43%) TFE reveal stable α-helices from Gly500 to Lys522, based on NH−NH$_{(i,i+1,2,3)}$, αH−NH$_{(i,i+2,3,4)}$, αH−βH$_{(i,i+3)}$, and weak αH−NH$_{(i,i+1)}$ NOEs. However, downfield shifts of the αH resonances from residues Gly500 to Ile507 and fewer intermediate-range NOEs suggest a less stable α-helix in the 25-mer even in saturating TFE. These findings show that the Phe508-containing region of CFTR has a propensity to form an α-helix, which is destabilized by the ΔF508 mutation found in most patients with CF. These studies have direct relevance to better understanding the CFTR misfolding problem associated with CF and to identifying chemical agents, which correct this problem.

Cystic fibrosis (CF) is an inherited disorder, which affects approximately 1 in 2000 people in the United States and Canada (*1*, *2*). The disease is characterized by lung infections, pancreatic insufficiency, and increased sweat Cl^- concentration. Individuals with severe cases of CF frequently die before the age of 30 as a result of chronic pulmonary infections with antibiotic-resistant bacteria. In approximately 70% of CF cases, a deletion of phenylalanine at position 508 in the cystic fibrosis transmembrane conductance regulator (CFTR[1]) is detected. The Phe508 residue resides in a portion of the sequence identified as the first of two nucleotide-binding folds (NBFs) or domains of CFTR (Figure 1), the overall structure of which consists of 5 domains (*3*): NBF1, NBF2, a regulatory (R) domain, and 2 transmembrane spanning domains (TMS1 and TMS2). CFTR is a member of a superfamily of proteins known as ABC (ATP-binding cassette) transporters (*4*) or traffic ATPases (*5*), and is believed to function physiologically as a Cl^- channel to help regulate conduction pathways for Cl^- and Na^+ in epithelial cells.

Deletion of Phe508 (ΔF508) from CFTR results in a protein that is unable to leave the endoplasmic reticulum (*6*) leading to its degradation (*7*, *8*). This blockage appears to be relieved if the ΔF508 mutant cells are grown at low temperatures (*9*) or in the presence of stabilizing agents such

[†] These studies were supported by NIH Grant DK28616 to A.S.M. and NIH Grants DK43962 and DK48977 to P.L.P. Y.H.K. was supported in part by the American Lung Association.

[‡] A complete listing of the distance restraints derived from NOE data have been deposited at the Brookhaven Protein Data Bank (Chemistry Department, Brookhaven National Laboratory, Upton, NY) (file names r1ckymr, r1ckzmr, r1ckxmr, and r1ckwmr, respectively) together with the atomic coordinates of the acceptable structures of P26 in H_2O (1cky), P25 in H_2O (1ckz), P26 in trifluroethanol (1ckx), and P25 in trifluroethanol (1ckw).

* To whom correspondence should be addressed. Phone: 410-955-2038. Fax: 410-955-5759. E-Mail: mildvan@welchlink.welch.jhu.edu.

[§] This author initiated the project.

[1] Abbreviations: CD, circular dichroism; CFTR, cystic fibrosis transmembrane conductance regulator; DQF−COSY, double quantum-filter correlated spectroscopy; DMSO-d_6, perdeuterated dimethyl sulfoxide; DIPSI, decoupling in the presence of scalar interaction; FID, free induction decay; NBF, nucleotide-binding fold; NMR, nuclear magnetic resonance; NOE, nuclear Overhauser effect; NOESY, NOE spectroscopy; P26, synthetic, 26-residue peptide with the sequence MPGTIKENII**F**GVSYDEYRYRSVIKA; P25, synthetic, 25-residue peptide lacking **F** but otherwise identical to P26; TFA, trifluoroacetic acid; TFE, trifluoroethanol; TPPI, time-proportional phase incrementation; TOCSY, total correlation spectroscopy; TSP, sodium 3-(trimethylsilyl)propionate-2,2,3,3,-d_4.

10.1021/bi9903603 CCC: $18.00
Published on Web 05/20/1999

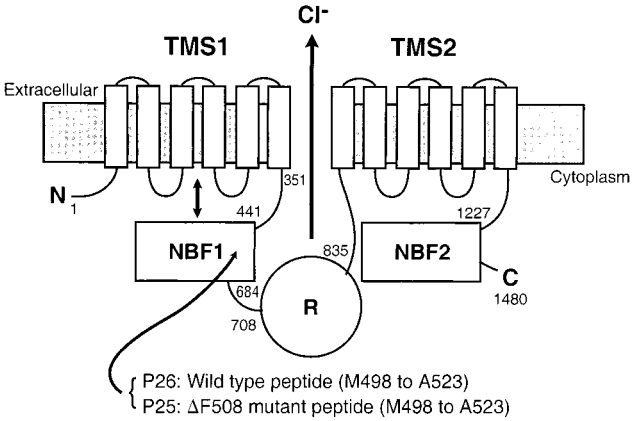

FIGURE 1: Model of CFTR. The model shows the two transmembrane-spanning domains (TMS1 and TMS2), the two nucleotide binding domains (NBF1 and NBF2), and the regulatory domain (R). The location of NBF1 peptides P25 and P26 used in this study is also indicated.

as glycerol or D_2O (*10*, *11*). It is believed, therefore, in support of an earlier hypothesis (*12*), based on circular dichroism (CD) and stability studies of long peptide segments (>60 amino acid residues) of NBF1 (*13*), that deletion of Phe508 leads to a misfolded protein which cannot be transported to the cell membrane. Significantly, more recent work has revealed that ΔF508 CFTR is functionally active within the endoplasmic reticulum (*14*), indicating that the "misfolded region", recognized by local quality control mechanisms responsible for the protein's retention, may be confined to a relatively small folding unit of the protein, namely, the ΔF508 region. Moreover, the expressed ΔF508 form of NBF1 shows significant structure and function, approaching that of wild-type NBF1 (*15*). These findings, together with recent 3-D modeling studies of NBF1 which predict that the critical Phe508 residue is located within a short α-helical region (*16*), provide a rational basis for better defining the folding defect in CF caused by the ΔF508 mutation. Consequently, a peptide (P26) corresponding to the predicted α-helical region containing Phe508 as defined by the 3-D modeling studies (*16*), as well as the same peptide lacking Phe508 (P25), were synthesized, and their solution structures were determined by ^{1}H NMR. A preliminary abstract of this work has been published (*17*).

EXPERIMENTAL PROCEDURES

Materials. The Vydac Protein & Peptide C_{18} column was obtained from Vydac Corp. Acetonitrile was obtained from Fisher Scientific and trifluoroacetic acid (TFA) from Applied Biosystems Inc. The solvent 2,2,2-trifluoroethanol-d_3 was obtained from Cambridge Isotope Laboratories and (dimethyl sulfoxide)-d_6 $(CD_3)_2SO$ from Aldrich. All other chemicals were of the highest purity commercially available.

METHODS

Peptide Synthesis and Purification. Both the 26-residue peptide (P26) consisting of Met498 to Ala523 and the 25-residue peptide (P25) lacking Phe508 were synthesized in the Johns Hopkins University Protein/Peptide facility on a PE Biosystems Model 430A Peptide Synthesizer. The solid-phase method of Merrifield (*18*) was used with F-moc (9-fluorenylmethoxycarbonyl) chemistry to protect α-amino groups. The peptides were purified using semipreparative HPLC chromatography utilizing a Vydac Protein & Peptide C_{18} (250 mm × 10 mm) column. Buffers consisted of 0.1% TFA in water and 0.08% TFA in acetonitrile. Following purification the complete amino acid sequences were verified in the same facility for each peptide with a PE Biosystems 492 Procise Protein Sequencer using Edman degradation Chemistry (*19*, *20*). Finally, the mass and purity of each peptide were verified by matrix-assisted UV laser desorption/ionization (MALDI) mass spectrometry in the Middle Atlantic Spectrometry Facility, located at Johns Hopkins University School of Medicine.

NMR Spectroscopy. The NMR samples consisted of 1.4 mM solutions of the 25-mer and 26-mer peptides in 90% H_2O/10%DMSO-d_6, pH 4.0. Identical NMR experiments were performed in 43% trifluoroethanol-d_3 (TFE) in H_2O, pH 4.0. All NMR experiments were recorded at 25 °C on a Varian UnityPlus 600 MHz spectrometer equipped with a pulse field gradient unit, four independent RF channels, and a Varian 5 mm triple resonance probe with an actively shielded *z*-gradient. The data were recorded using the States-TPPI method (*21*) in all indirect dimensions, with a relaxation delay of 1.5 s. Water suppression for the NOESY (*22*, *23*) and TOCSY (*24*, *25*) experiments was achieved with a WATERGATE pulse train (*26*) attached at the end of each pulse sequence immediately before data acquisition.

The 2D NOESY spectra were collected as follows: 100, 200, and 300 ms mixing times, spectral widths of 5500 Hz (^{1}H, t_1, 1024 complex points) and 5500 Hz (^{1}H, t_2, 2048 complex points), and 64 transients per hypercomplex t_1,t_2 pair. The 2D TOCSY spectra of the peptides were collected with otherwise identical parameters but with a 65 ms spinlock time using the DIPSI-2 (*27*) pulse train. The 2D DQF−COSY spectra were collected with spectral widths of 6000 Hz (^{1}H, t_1, 1024 complex points) and 6000 Hz (^{1}H, t_2, 2048 complex points) and 64 transients per hypercomplex t_1,t_2 pair. Water suppression for the DQF−COSY was obtained with a 1.5 s presaturation pulse.

Data Processing. The NMR data were processed on an Indigo^{2}XZ Silicon Graphics workstation using the Felix 2.3 software package (Biosym Technologies). All of the spectra were processed similarly by first applying a convolution Gaussian window function of 16 to the FIDs to artificially remove the water resonance, then applying a 75°-shifted sinebell square (ss) window function to the 1024 points of the FIDs, followed by Fourier transformations and polynomial baseline corrections. Apodization with an 80°-sinebell-shifted window function was applied followed by zero-filling in the t_1 dimension to 1024 points to yield final matrix sizes of 1024 (f_1) × 1024 (f_2) real data points. The observed ^{1}H chemical shift was referenced with respect to the H_2O signal, which was taken as 4.773 ppm downfield from external TSP at 25 °C. Subsequent data analysis including measurements of intensities of $\alpha H-NH_{(i,i+1)}$ and $NH-NH_{(i,i+1)}$ NOEs was done using the NMRVIEW 2.1 software package (*28*).

Structural Calculations. Distance restraints of 1.8−2.8, 1.8−3.2, and 1.8−5.0 Å were employed for NOE cross-peaks of strong, medium, and weak intensity, respectively, observed in the 2D ^{1}H−NOESY spectra obtained with 200 ms mixing times. An additional 1.0 Å was added for NOEs involving methyl protons, and a correction of 2.3 Å was added to restraints for NOEs involving degenerate Hδ or Hϵ protons

of the tyrosines and phenylalanine. For the structures presented here, no hydrogen bond or dihedral angle restraints were employed.

Distance geometry, simulated annealing, and refinement calculations were performed with X-PLOR 3.8 (*29*) operating on an 8-processor Silicon Graphics R10000 Power Challenge computer. All atoms of the 25- and 26-residue peptides were included in the structure calculations. For both the 25-mer and the 26-mer in H_2O and in TFE, a set of 50 embedded substructures was generated using distance geometry and regularized by energy minimization against a distance geometry energy term (the sub-embed protocol in X-PLOR). After template fitting, the embedded substructures were further regularized by simulated annealing with a starting temperature of 1000 K and using 2000 steps in both the annealing and the cooling stages with a time-step of 1 fs. The resulting structures underwent a simulated annealing refinement of the slow-cooling type with a starting temperature of 2000 K and 1000 steps during the cooling stage with a time-step of 1 fs, followed by 500 steps of energy minimization. During the refinement, the nonbonded interactions were modeled only by a quadratic repulsive energy term, while the attractive components of the Lennard-Jones potential and the electrostatic energy were turned off. At the final stages of refinement, a square-well potential energy function was used for the NOEs with a force constant of 50 kcal mol^{-1} $Å^{-2}$. Of the 50 embedded substructures, 40 converged to acceptable structures with NOE violations $\leq$0.35 Å. Of these, the best structures with NOE violations $\leq$0.35 Å and total energies $\leq$70 kcal/mol were selected. Superpositioning of computed structures and calculations of rmsd values were performed with the MidasPlus software package.

RESULTS

Establishment of Conditions for NMR Studies. The NMR solution studies of both the 26- and 25-mer peptides were performed with 10% DMSO-d_6 in H_2O at pH 4.0 and 25 °C because these peptides tended to form a highly viscous solution over time in D_2O, and to become much less soluble at higher pH. Ten percent deuterated DMSO in H_2O was therefore selected for both P26 and P25 because the peptides appeared to be both stable and highly soluble in this solvent mixture at pH 4.0. The deuterated DMSO also provided a deuterium lock for the NMR samples.

NMR Analysis of the Structure of P26 in H_2O, 10% DMSO. The assignments of the backbone and side chain proton resonances of P26 were made from the 2D NOESY and TOCSY spectra collected at 200 and 65 ms mixing times, respectively. Well-resolved NH$-$NH$_{(i,i+1)}$ and αH$-$NH$_{(i,i+1)}$ sequential NOEs (Figure 2) provided unambiguous connectivities from Pro499 to Lys522. Due to exchange broadening, the NH and αH resonances of amino-terminal Met498 and carboxyl-terminal Ala523 were not observed, precluding the assignment of their side chain proton resonances. The side chain proton resonances of all other residues were unambiguously identified from the 2D TOCSY (Figure 3). In addition, only a limited number of medium-range (i, $i + 2$, and i, $i + 3$) NOEs were observed, and no αH$-$NH$_{(i,i+4)}$ or αH$-\beta$H$_{(i,i+3)}$ NOEs between sequential residues were detected. The assignment of the amino acid type was also aided

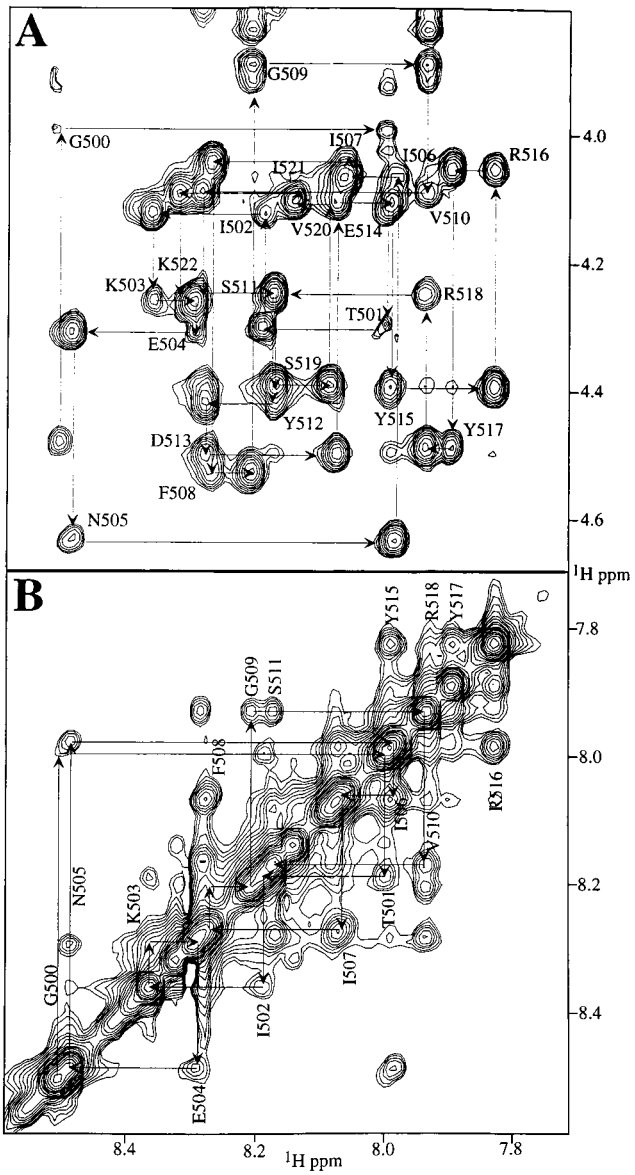

FIGURE 2: Two regions of the 2D NOESY spectrum of P26 in H_2O and 10% DMSO-d_6 collected with a mixing time of 200 ms. (A) αH$-$NH$_{(i,i+1)}$ NOE connectivities for residues Pro499 to Lys522. (B) NH$-$NH$_{(i,i+1)}$ NOE connectivities only for residues Gly500 to Ser511 are shown for simplicity; in addition, Tyr515 to Arg518 are labeled.

by the presence of aromatic residues in the sequence which have distinct δH and ϵH shifts. The assignments of the ^{1}H resonances of P26 in H_2O are given in Table S1 of Supporting Information.

Based on the intense NH$-$NH$_{(i,i+1)}$ and αH$-$NH$_{(i,i+1)}$ sequential NOEs (Figure 2) and the lack of medium-range sequential NOEs, P26 appears to form a continuous but labile helix. The intensities of the NOEs providing the NH$-$NH$_{(i,i+1)}$ connectivities between Gly500 and Ile521 are on average 57% of the intensities of the αH$-$NH$_{(i,i+1)}$ NOEs. If the peptide assumed uniform conformations, then this value would suggest that it resides in an extended conformer 64% of the time and in a helix 36% of the time, although these are approximations. However, on the basis of the presence of i, $i + 2$, and i, $i + 3$ NOEs, it appears that residues Tyr512 to Lys522 exist in a more stable helical conformation than do residues of the preceding half of the protein (Figure 4A).

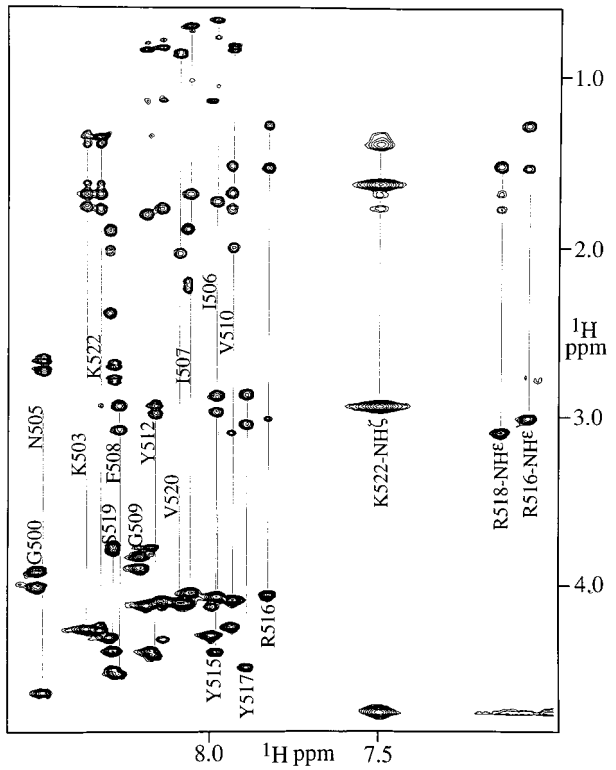

FIGURE 3: Portion of the 2D TOCSY spectrum showing the fingerprint region (NH protons to side chain proton correlations) of P26 in H_2O. Lines are drawn between the resonances corresponding to the intraresidue protons for all of the amino acid residues except for the terminal residues, Met498 and Ala523.

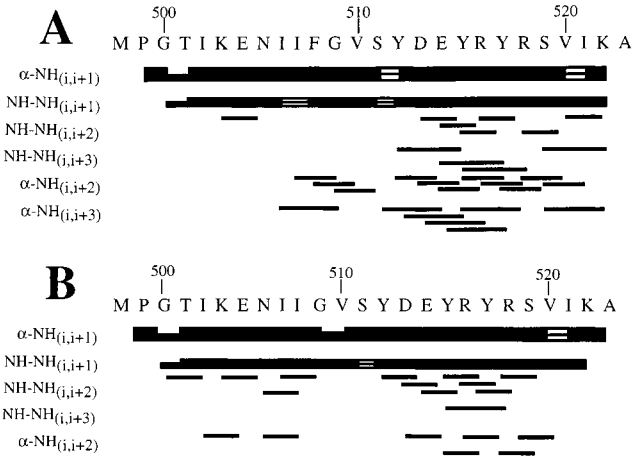

FIGURE 4: Diagram summarizing near-neighbor NOEs. (A) P26 and **(**B**)** P25 in H_2O, 10% DMSO-d_6 using NOEs from the 200 ms mixing time 2D NOESY spectra. The heights of the bars indicate NOE intensities as either strong, medium, or weak.

NMR Analysis of the Structure of P25 in H_2O, 10% DMSO. The NMR spectra of the P25 peptide were collected using the same parameters as with P26. The ^{1}H chemical shifts of P26 and P25 were different, requiring completely independent assignment of the resonances and sequential connectivities of P25. Well-resolved signals in the amide proton and the alpha proton regions of the 2D NOESY spectra of P25 provided unambiguous NH−NH$_{(i,i+1)}$ and αH−NH$_{(i,i+1)}$ NOE connectivities from Pro499 to Ala523 (Figure 5). The NH and αH resonances of the amino-terminal Met498 were not observed, precluding the assignment of its other resonances. The assigned amide NH resonances of Ser511 and

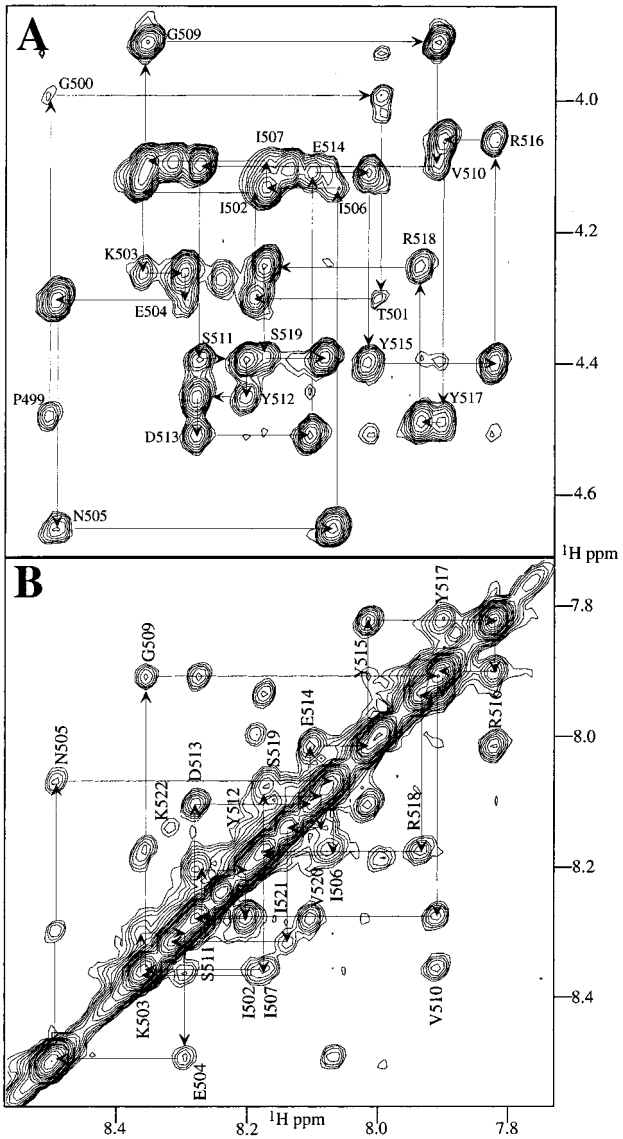

FIGURE 5: Two regions of the 2D NOESY spectrum of P25 in H_2O and 10% DMSO-d_6 collected with a mixing time of 200 ms. (A) αH−NH$_{(i,i+1)}$ NOE connectivities for residues Gly500 to Val520, and (B) NH−NH$_{(i,i+1)}$ NOE connectivities for residues Ile502 to Lys522 are drawn.

Tyr512 and of Lys522 and Ala523 were close to the diagonal. Hence unambiguous sequential connectivities for these pairs of residues were determined from αH−NH$_{(i,i+1)}$ NOEs, which also established their NH−NH$_{(i,i+1)}$ connectivities. In a similar manner, the αH resonances of Val520 and Ile521 overlapped and definitive connectivity between these residues was provided by the NH−NH$_{(i,i+1)}$ NOEs. The side chain proton resonances of all amino acid residues were easily identified in the 2D TOCSY which were well-resolved (data not shown). Like the backbone connectivities of P26, no αH−NH$_{(i,i+4)}$ or αH-βH$_{(i,i+3)}$ NOEs were observed for P25 (Figure 4B). The assignments of the ^{1}H resonances of P25 in H_2O are given in Table S2 of Supporting Information.

As found with P26, P25 also forms a continuous but labile helix in H_2O. The intensities of the NH−NH$_{(i,i+1)}$ NOEs of P25 are on average 51% of the intensities of the αH−NH$_{(i,i+1)}$ NOEs between residues Gly500 and Val520, suggesting that if the peptide were to assume uniform conformations, it would be in an extended conformation 66% of the time and

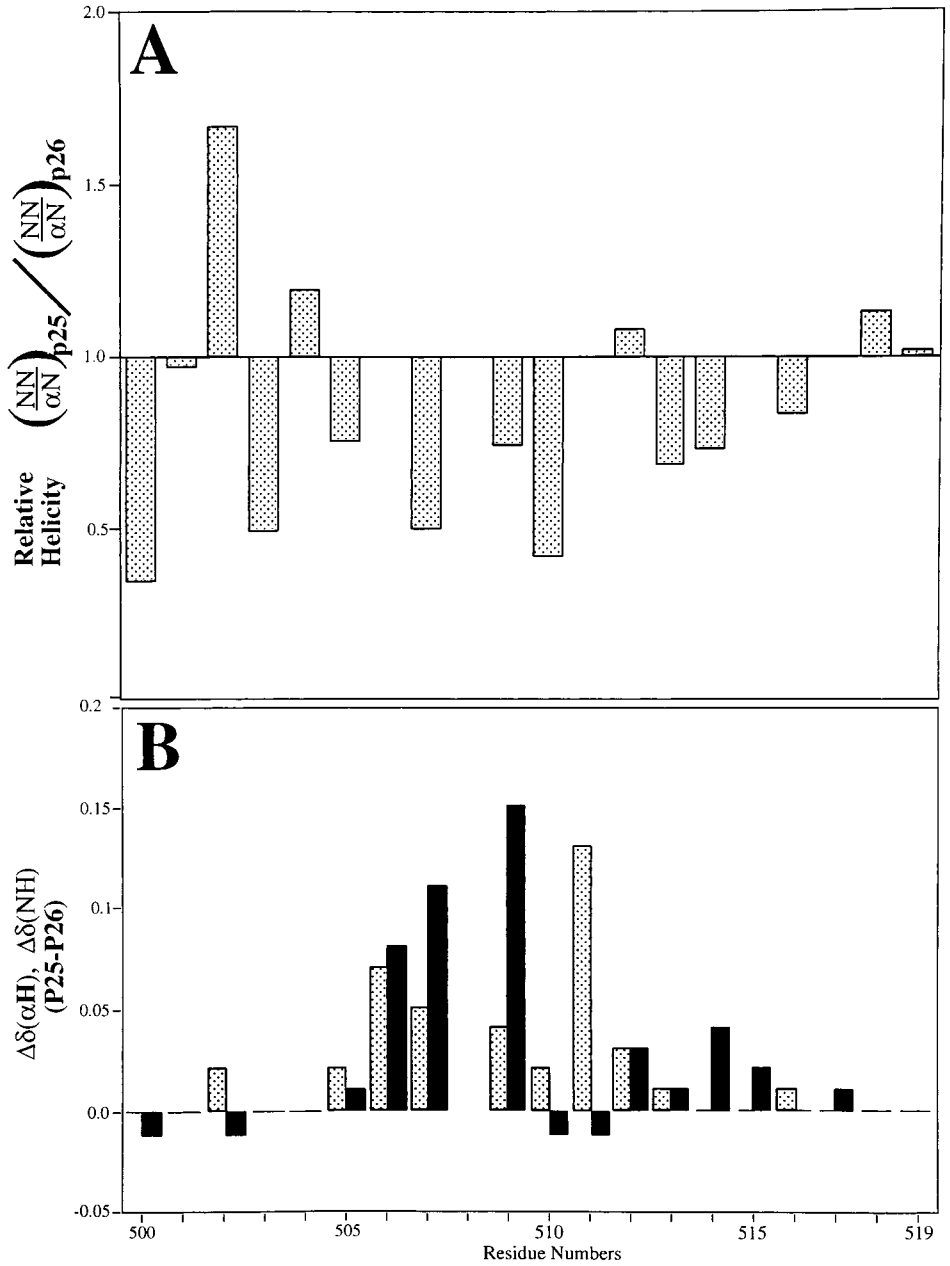

FIGURE 6: Comparison of the helical propensities of P25 relative to P26. (A) Plotted are the intensity ratios of the ($NH-NH_{(i,i+1)}/\alpha H-NH_{(i,i+1)}$) NOEs of P25 relative to those of P26 for residues Gly500 to Val520 obtained from the 200 ms NOESY spectra. The ratios are plotted relative to 1, which indicates identical helical propensities in both peptides. (B) Differences in chemical shifts between P25 and P26 for the αH resonances (stippled bars) and NH resonances (filled bars) of residues Gly500 to Val520. Corresponding residues of P25 and P26 are aligned.

in a helix 34% of the time, although these are approximations. However, as in P26, residues Tyr512 to Val520 of P25 appear to form a more stable helical structure than do residues Gly500 to Ser511 (Figure 4).

Helical Propensities of P25 and P26 in H_2O. A lower helical propensity of P25 compared to P26 in H_2O is indicated by the detection of 21 intermediate-range NOEs characteristic of helices in P25 in comparison with 29 such NOEs in P26 (Figure 4). Because both P25 and P26 form labile helices in equilibrium with extended conformations (Figure 4), a quantitative estimate of relative contributions of helical to extended conformation for each residue in the two peptides was obtained from the ratios of the integrated intensities of the sequential $NH-NH_{(i,i+1)}/\alpha H-NH_{(i,i+1)}$ NOEs (Figure 6A). In Figure 6A, a region of decreased helicity in P25 relative to that in P26 is seen from residues 505−514, surrounding the missing residue, Phe508. The average ratio of $NH-NH_{(i,i+1)}/\alpha H-NH_{(i,i+1)}$ NOEs of the 25-mer in comparison with the 26-mer in this region is 0.707 ± 0.158, indicating that the helical propensity of the 25-mer is 71% of that of the 26-mer between residues 505 and 514.

Independent evidence for a decrease in helical propensity in P25 surrounding the missing residue is the downfield chemical shifts of the αH and NH resonances of P25 compared to those of P26 from residues 505 to 517 (Figure 6B) (*30*). For the αH resonances the average $\Delta\delta$ over this region is 0.05 ppm and the range is 0.02−0.13 ppm. For the NH resonances, the average $\Delta\delta$ is 0.037 ppm and the range is −0.01 to 0.15 ppm. Although these small changes could

Table 1: NMR Restraints and Structural Statistics for the P26 and P25 Peptides in H_2O and TFE

	P26 (H_2O)	P25 (H_2O)	P26 (TFE)	P25 (TFE)
X-PLOR Input NOE Restraints				
sequential ($\|i - j\| = 1$)	112	95	132	92
intraresidue	170	143	170	149
medium range ($1 < \|i - j\| \leq 5$)	40	20	101	66
total NOEs	322	258	403	307
NOEs/residue	12.4	10.3	15.4	10.3
Average RMSD from Idealized Geometry of Each Set of Structures				
bonds (Å $\times 10^{-3}$)	$2.92 \pm 2.01 \times 10^{-4}$	$1.95 \pm 1.50 \times 10^{-4}$	$2.11 \pm 2.04 \times 10^{-4}$	$1.98 \pm 1.04 \times 10^{-4}$
angles (deg $\times 10^{-1}$)	$4.04 \pm 5.04 \times 10^{-2}$	$3.46 \pm 1.76 \times 10^{-2}$	$3.51 \pm 1.09 \times 10^{-2}$	$3.43 \pm 1.08 \times 10^{-4}$
improp. (deg $\times 10^{-1}$)	$2.79 \pm 2.55 \times 10^{-2}$	$2.60 \pm 1.34 \times 10^{-2}$	$2.58 \pm 1.98 \times 10^{-2}$	$2.89 \pm 2.05 \times 10^{-4}$
Pairwise RMSD of the Ensemble of Calculated Structures (Å)[a]				
backbone, 2° structure[b]	5.67 ± 1.29	5.09 ± 1.26	1.61 ± 0.62	1.25 ± 0.27
all atoms, 2° structure	7.82 ± 1.07	7.48 ± 1.16	2.89 ± 0.69	2.59 ± 0.27
backbone, M498-A523	6.97 ± 1.76	6.07 ± 1.51	2.42 ± 0.85	2.49 ± 0.55
all atoms, M498-A523	8.74 ± 1.37	7.69 ± 1.33	3.63 ± 0.93	3.60 ± 0.48

[a] The pairwise root-mean-square deviations (rmsd) of 10 and 27 computed structures for the P26 and P25 peptides, respectively, in H_2O, 10% DMSO-d_6 were superimposed. For both P26 and P25 in TFE, 13 computed structures were superimposed. [b] Residues superimposed for all of the structures are Thr504 to Lys522 where secondary structure is found in 43% TFE.

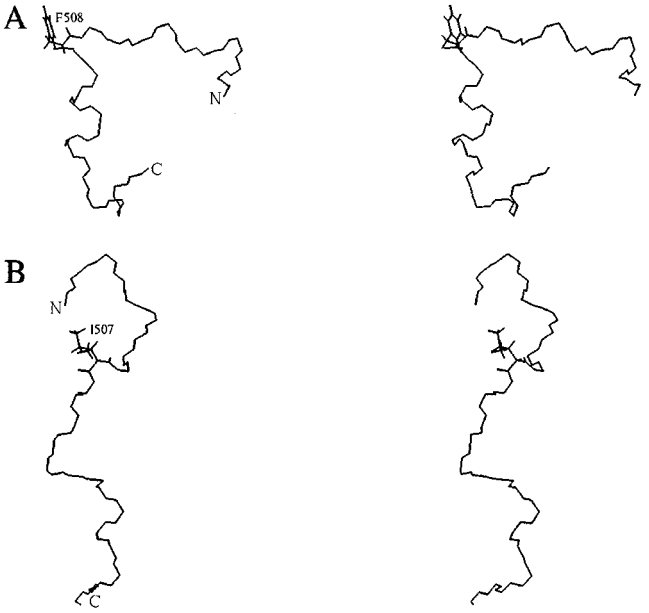

FIGURE 7: Lowest-energy structures of P26 (A) and P25 (B) in H_2O, 10% DMSO-d_6 shown as stereopairs. The side chain of Phe508 is shown in P26, and this side chain of Ile507 is shown in P25.

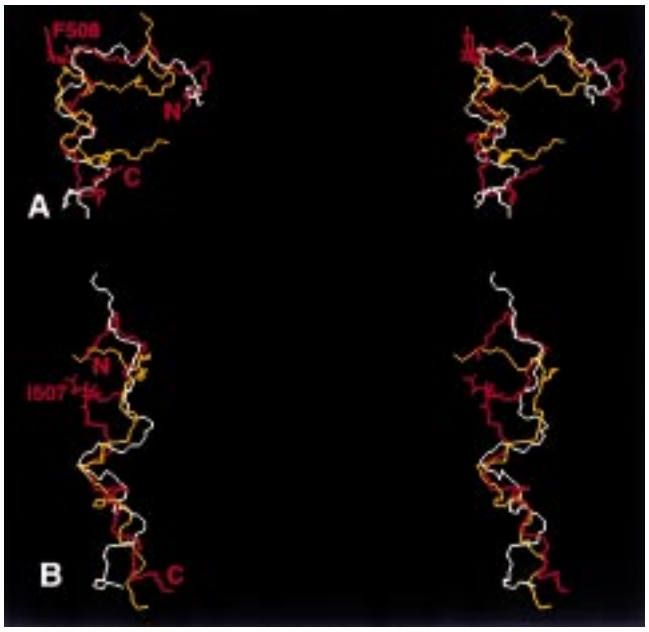

FIGURE 8: Ranges of structures of P26 (A) and P25 (B) in H_2O, 10% DMSO-d_6, shown as stereopairs. The lowest-energy structure is shown in red with the Phe508 side chain, and the two most different acceptable structures are shown in amber and white. The backbone atoms of Thr501−Lys522 are superimposed.

have resulted in part from the loss of ring current shielding by Phe508, their uniform direction argues against this being the sole explanation.

Computed Structures of P26 and P25 in H_2O. For P26, 10 of the 50 computed structures had no NOE violations greater than 0.35 Å and were of low energy (Table 1). While all of the structures showed helicity between residues Phe508 and Tyr517, they did not superimpose well (Table 1) as is generally found for peptides. Figure 7A shows the lowest-energy structure of P26 in H_2O, and Figure 8A shows the two most different acceptable structures superimposed onto the lowest-energy structure.

For P25, 27 of the 50 computed structures were acceptable by the above criteria, and also did not superimpose well (Table 1). Figure 7B shows the lowest-energy structure of P25 in H_2O, and Figure 8B shows the two most different acceptable structures superimposed onto the lowest-energy structure. While some turns were present in P25, all of the structures of P25 showed much less helicity than those of P26 in H_2O, confirming the analysis of the primary NMR data.

Comparison of P26 and P25 in TFE. The structures of P26 and P25 were also determined in trifluoroethanol, a solvent known to promote helix formation of small polypeptides which have helix-forming propensities (*31*). Preliminary CD titrations of both P26 and P25 with TFE showed progressive decreases in molar ellipticity at 222 nm indicative of helix formation, with no further changes above 33% TFE (*17*). Accordingly, 43% TFE, deuterated to permit field/frequency locking, was used for the NMR studies of both peptides. In 43% TFE, the NMR data indicate that both P25 and P26 form stable α-helices between residues Gly500 and Lys522. Backbone proton connectivities were assigned via high-intensity NH−$NH_{(i,i+1)}$ and weak- to medium-intensity αH−$NH_{(i,i+1)}$ NOEs (Figure 9). In addition, extensive

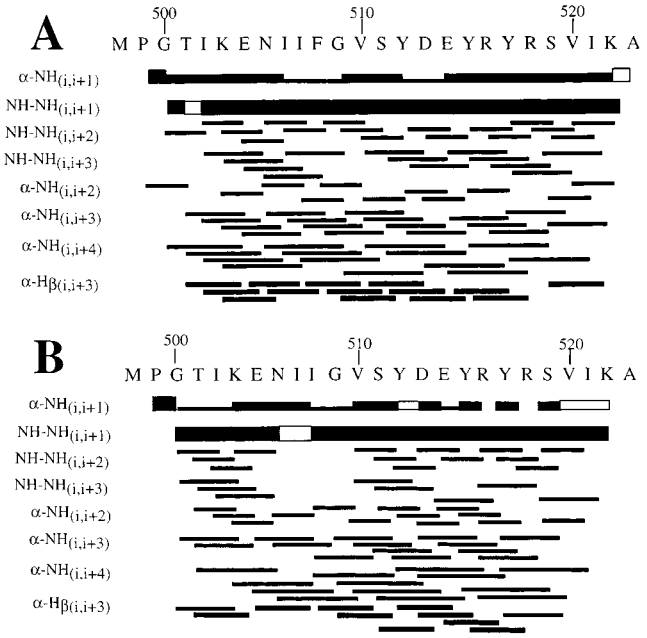

FIGURE 9: Diagram summarizing near-neighbor NOEs. (A) P26 and (B) P25 in 43% TFE using NOEs from the 200 ms mixing time 2D NOESY spectra. The heights of the bars indicate NOE intensities as either strong, medium, or weak.

intermediate-range NH−$NH_{(i,i+2,3)}$, αH−$NH_{(i,i+2,3,4)}$, and αH-$\beta H_{(i,i+3)}$ NOEs were observed (Figure 9) consistent with both peptides existing in stable α-helical conformations. The chemical shifts of the αH resonances as well as the relative intensities of the sequential NH−$NH_{(i,i+1)}$ to αH−$NH_{(i,i+1)}$ NOEs are also consistent with residues Gly500 to Lys522 being in an α-helix. The NH and αH resonances of the amino-terminal Met498 in both peptides were not observed. Hence its connectivities to Pro499 could not be established. The NH proton of the carboxy-terminal Ala523 was observed in P26 but not in P25. The assignments of the ^{1}H resonances of P26 and P25 in 43% TFE are given in Tables S3 and S4, respectively, of Supporting Information.

A comparison of the αH chemical shifts of P25 and P26 in 43% TFE indicates that the deletion of Phe508 deshields the αH resonances of the preceding residues Gly500 to Ile507 but does not significantly affect those of Tyr512 to Lys522. The αH resonance of Ile507 is the most deshielded, by 0.32 ppm, while residues Asn505 to Lys522 show varying degrees of deshielding (0.09−0.31 ppm). However, the αH resonance of Thr501 is highly shielded, shifting upfield by 0.35 ppm. While these changes may result in part from the loss of ring current effects of Phe508, they may also reflect a subtle change in the peptide backbone conformation. The NH shifts, which are less sensitive to changes in the backbone conformation than the αH shifts, do not show significant differences between corresponding residues of the two peptides, arguing against significant ring current effects of Phe508. The downfield direction of most of the changes in the αH chemical shifts of residues Gly500 to Ile507 of P25 toward random coil values, as well as the fewer intermediate-range NOEs of P25 (Figure 9, Table 1), suggest that this region of P25 may not form as stable an α-helix as does the corresponding region of P26, even at a high concentration of TFE.

Computed Structures of P26 and P25 in TFE. For both P26 and P25 in TFE, 13 of the 50 computed structures were acceptable and converged well (Table 1). Both P26 and P25 showed well-defined α-helices from Thr501 to Lys522 (Figure 10), which were superimposable onto each other with an rmsd of 2.60 ± 0.58 Å for the backbone atoms (Figure 11).

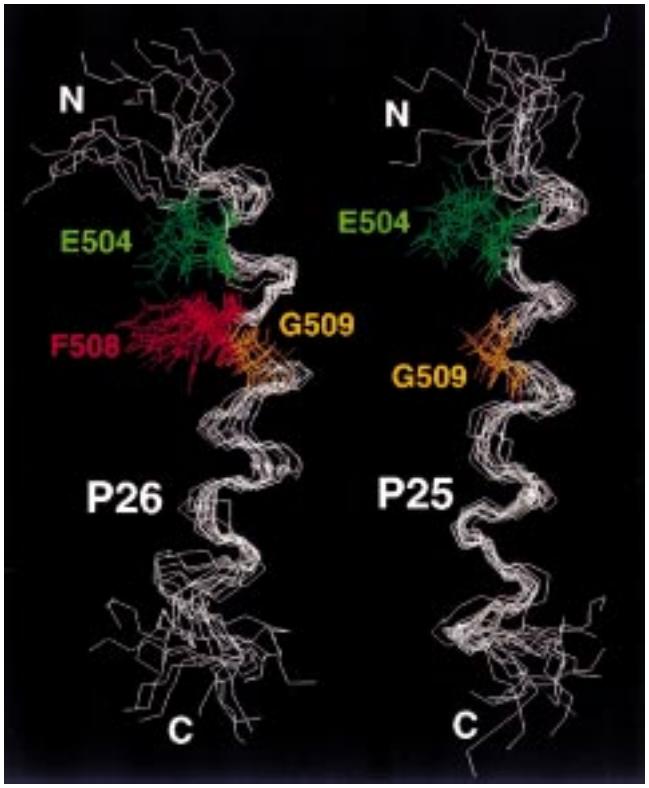

FIGURE 10: Solution structures of P26 (left) and P25 (right) in 43% TFE. In each case, the backbone atoms of 13 acceptable structures are superimposed from residues Thr501 to Lys522. Also shown are the side chains of Glu504, Phe508, and Gly509.

DISCUSSION

The peptide P26 consists of residues 498−523 within the first nucleotide-binding fold (NBF1) of wild-type CFTR, while P25 lacks Phe508 but is otherwise identical to P26, thus mimicking the predominant mutation found in CF. The studies reported here show that in the "wild-type" peptide, Phe508 lies within a helical region. In addition, three independent observations indicate a significant decrease in the helix-forming propensity of P25 in comparison with P26 in H_2O. First, the relative intensity ratios of the sequential NH−$NH_{(i,i+1)}$/αH−$NH_{(i,i+1)}$ NOEs, a measure of the helical/extended contributions to conformation, are significantly lower (0.707 ± 0.158) for residues 505−514 of P25 than for the corresponding residues of P26 (Figure 6A). Second, P26 shows 29 intermediate-range NOEs characteristic of helices while P25 shows only 21 (Figure 4). Third, in H_2O, significant downfield chemical shifts of the αH and NH resonances of residues 505−517 occur in P25 in comparison with those of P26, consistent with a lower helicity of P25 in the region surrounding the missing residue (Figure 6B). This difference in helical propensity is confirmed by the computed NMR structures of P26 and P25 in H_2O (Figures 7, 8).

The lower helicity of P25 compared to P26 in H_2O is noteworthy since P25 lacks a phenylalanine, a residue with an unfavorable intrinsic helix-forming propensity of +0.67

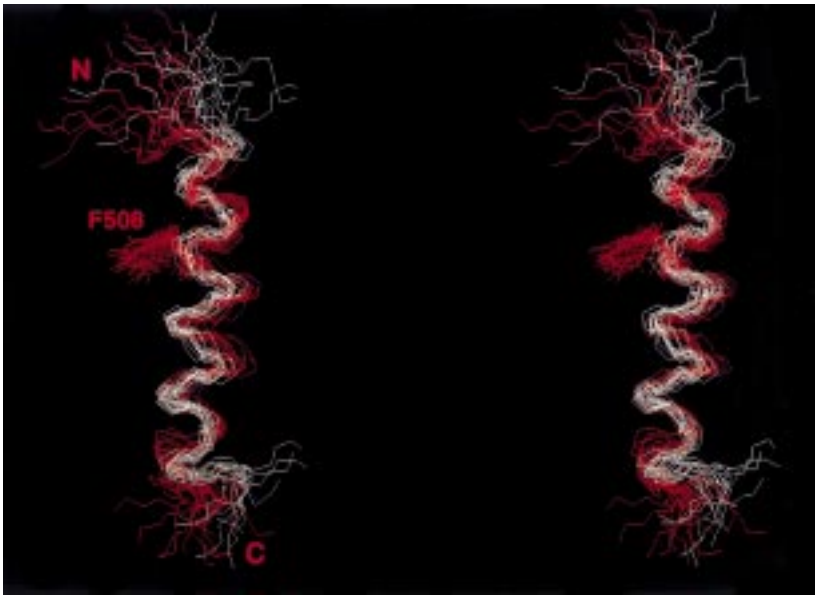

FIGURE 11: Comparison in stereo of the structures of P26 and P25 in 43% TFE. The backbone atoms of 13 acceptable structures of both P26 and P25 are superimposed from residues Thr501 to Ile507, and from Gly509 to Lys522. P26 is in red showing the side chain of Phe508, and P25 is in white.

kcal/mol in ala-rich peptides (*32*). Helical regions of peptides and proteins containing phenylalanine residues are believed to be stabilized by side chain interactions (*32*). Hence, the loss of side chain interactions involving Phe508 may destabilize the helix in P25. This explanation is supported by the region of decrease in helicity of P25 in H_2O, between residues 505 and 517, which surrounds position 508.

In TFE, both P26 and P25 form α-helices from residues Thr501 to Lys522 (Figures 10, 11), which may mimic the folded state of this region in intact CFTR. Although the P25 ΔF508 "mutant" peptide forms an α-helix in TFE, it may be less stable between residues Gly500 and Ile507 based on chemical shift and NOE criteria (Table 1). However this difference is not apparent in the computed NMR structures of P25 and P26 (Figure 11). The α-helical structure of P26 in TFE reveals a hydrophobic i to $i + 4$ side chain−side chain interaction between Glu504 and Phe508, which may contribute to the net stabilization of the helix by Phe508 (Figure 10, left). In P26, a weak NOE is found between Phe508 δH and Glu504 βH indicating the proximity of these two residues in the α-helical form of this peptide. Such proximity in intact CFTR would also provide a hydrophobic environment, which would increase the pK_a of Glu504.

It is of interest to compare work reported here on the "wild-type" P26 and "mutant" P25 CFTR peptides (Met498 to Ala523) using NMR with those conducted earlier on "wild-type" P67 and "mutant" ΔF508 P66 peptides using CD (*13*). In the latter study that included CFTR residues Arg450 to Arg516, the data were consistent with a location of F508 within a β-sheet region in P67 that became unstable in P66 resulting in random coil formation. Significantly, both studies emphasize the importance of F508 for structural stability in this critical region of CFTR. The differences in secondary structure may reflect either different conditions used in the two studies (i.e., 90% H_2O/10% DMSO, pH. 4.0, in this study versus 100% H_2O, pH 5.5, in the earlier study) or that in the earlier studies the P67 and P66 peptides lacked 7 amino acids (Tyr517 to Ala523) at their C-termini. These amino acids which are present in the P25 and P26 peptides used in the present study are predicted from 3-D modeling studies (*16*) to contain the entire α-helical region of CFTR that includes Phe508. It has long been known that truncations of helices can destablize them (*33*). Relevant to the conclusion derived from the current study is a recent 1.5 Å X-ray structure of the HisP protein (*34*), the ATP-binding subunit of the histidine permease, which like CFTR is a member of the ABC transporter superfamily (*4*, *5*). Thus, in the X-ray structure of HisP at 1.5 Å resolution, the region believed to correspond to the F508 region in CFTR is an α-helix in agreement with 3D modeling studies based on the structures of F1 ATPase and the RecA protein (*16*).

The studies reported here are the first to provide evidence that the Phe508 region of CFTR has a propensity to form an α-helix in solution and that deletion of this single aromatic residue destabilizes the helix. These findings may be very relevant to earlier findings that, in CF caused by the ΔF508 mutation, ΔF508 CFTR is retained in the endoplasmic reticulum (*6*) and targeted for degradation (*7*, *8*). Thus, the structural changes noted here that occur upon deletion of Phe508 may prevent CFTR from undergoing the conformational transition believed to be essential for its normal trafficking to the plasma membrane (*35*) while alerting the quality control proteins which target the mutant protein for degradation (*7*, *8*).

Significantly, recent studies (*10*, *11*) have shown that a number of chemiosmolytes known to stabilize proteins can promote normal trafficking of ΔF508 CFTR to the plasma membrane where it becomes functional, at least in part. Although it is assumed that these chemiosmolytes or "chemical chaperones" as they are also called (*10*, *11*), correct a misfolding problem within the ΔF508 region, this possibility has never been demonstrated directly. Therefore, the P26 and P25 peptides, which are representative respectively of the Phe508 and ΔF508 regions of the wild-type and ΔF508 CFTR proteins, may serve as a model system for testing this hypothesis, and as the basis of a simple in vitro assay for selecting other chemical agents that correct the structural defect caused by the ΔF508 mutation. Work to be reported

elsewhere shows by CD spectroscopy that 10% D_2O increases the helicity of P25. In intact cells containing the ΔF508 mutation of CFTR, D_2O has been shown to facilitate the trafficking of ΔF508 CFTR from the endoplasmic reticulum, where it was trapped, to the plasma membrane (*10*).

ACKNOWLEDGMENT

We would like to thank Drs. Barbara Amman and Apo Gittis for their suggestions and help with the X-PLOR calculations.

SUPPORTING INFORMATION AVAILABLE

Four tables (Tables S1−S4) giving the ^1H resonance assignments of P26 and P25 in H_2O/10% DMSO-d_6 (S1 and S2, respectively) and in 43% TFE (S3 and S4, respectively) are available. This material is available free of charge via the Internet at http://pubs.acs.org.

REFERENCES

1. Welch, M. J., Tsui, L.-C., Boat, T. F., and Beaudet, A. L. (1995) in *The Metabolic and Molecular Bases of Inherited Diseases* (Scriver, C. R., Beaudet, A. L., Sly, W. S., and Valle, D., Eds.) pp 3799−3876, McGraw-Hill, Inc.
2. Ramsey, B. W. (1996) *New Eng. J. Med. 335*, 179−188.
3. Riordan, J. M., Rommens, J. M., Kerem, B. S., Alon, N., Rozmahel, R., Grzlvzak, Z., Zeilenski, J., Lok, S., Plasvsic, N., Chou, J., Drumm, L., Iannuzzi, M. L., Collins, F. S., and Tsui, L. C. (1989) *Science 245*, 1066−1073.
4. Higgins, C. F. (1992) *Annu. Rev. Cell. Biol. 8*, 67−113.
5. Doige, C. A., and Ferro-Luzzi Ames, G. (1993) *Annu. Rev. Microbiol. 47*, 291−319.
6. Cheng, S. H., Gregory, R. J., Marshall, J., Paul, S., Souza, D. W., White, G. A., O'Riordan, C. R., and Smith, A. E. (1990) *Cell 63*, 827−834.
7. Ward, C. L., Omura, S., and Kopito, R. R. (1995) *Cell 83*, 121−127.
8. Jensen, T. J., Loo, M. A., Pind, S., Williams, D. B., Goldberg, A. L., and Riordan, J. R. (1995) *Cell 83*, 129−135.
9. Denning, G. M., Anderson, M. P., Amara, J. F., Marshall, J., Smith, A. E., and Welsh, M. J. (1992) *Nature 358*, 761−764.
10. Brown, C. R., Hong-Brown, L. W., Biwersi, J., Verkman, A. S., and Welch, W. J. (1996) *Cell Stress*, Chapter 1, pp 117−125.
11. Sato, S., Ward, C. L., Krouse, M. E., Wine, J. J., and Kopito, R. R. (1996) *J. Biol. Chem. 271*, 635−638.
12. Thomas, P. J., Ko, Y. H., and Pedersen, P. L. (1992) *FEBS Lett 312*, 7−9.
13. Thomas, P. J., Shenbagamurthi, P., Sondek, J., Hullihen, J. M., and Pedersen, P. L. (1992) *J. Biol. Chem. 267*, 5757−5730.
14. Pasyk, E. A., and Foskett, J. K. (1995) *J. Biol. Chem. 270*, 12347−12350.
15. Ko, Y. H., Thomas, P. J., Delannoy, M. R., and Pedersen, P. L. (1993) *J. Biol. Chem. 268*, 24330−24338.
16. Bianchet, M. A., Ko, Y. H., Amzel, L. M., and Pedersen, P. L. (1997) *J. Bioenerg. Biomembr. 29*, 503−523.
17. Massiah, M. A., Ko, Y. H., Pedersen, P. L., and Mildvan, A. S. (1999) in *42nd Annual Meeting of the Biophysical Society*, *Biophys. J. 76*, A428, Abs. W-Pos-155.
18. Merrifield, R. B. (1963) *J. Am. Chem. Soc. 85*, 2149−2154.
19. Edman, P. (1950) *Acta Chem. Scad. 4*, 283−293.
20. Hunkapillar, M. W., and Hood, L. E. (1983) *Science 219*, 650−659.
21. Marion, D., Driscoll, P. C., Kay, L. E., Wingfield, P. T., Bax, A., Gronenborn, A. M., and Clore, G. M. (1989) *Biochemistry 28*, 6150−6156.
22. Jeener, J., Meier, B. H., Bachmann, P., and Ernst, R. R. (1979) *J. Chem. Phys. 71*, 4546−4553.
23. Macura, S., and Ernst, R. R. (1980) *Mol. Phys. 41*, 95−117.
24. Braunschweiler, L., and Ernst, R. R. (1983) *J. Magn. Res. 53*, 521−528.
25. Davis, D. G., and Bax, A. (1985) *J. Am. Chem. Soc. 107*, 2820−2821.
26. Piotto, M., Saudek, V., and Sklenar, V. (1992) *J. Biomol. NMR 2*, 661.
27. Shaka, A. J., Lee, C. J., and Pines, A. (1988) *J. Magn. Res. 77*, 274−293.
28. Johnson, B. A., and Blevins, R. A. (1994) *J. Biomol. NMR 4*, 603.
29. Brunger, A. T. (1992) X-PLOR (Version 3.1), A System for X-ray Crystallography and NMR, Yale University Press, New Haven, Connecticut.
30. Wishart, D. S., and Sykes, B. D. (1991) *J. Mol. Biol 222*, 311−333.
31. Dyson, H. J., and Wright, P. E. (1993) *Curr. Opin. Struct. Biol. 3*, 60−65.
32. Chakrabartty, A., Kortemme, T., and Baldwin, R. L. (1994) *Protein Sci. 3*, 843−852.
33. Fry, D. C., Byler, M., Susi, H., Brown, E. M., Kuby, S. A., and Mildvan, S. A. (1988) *Biochemistry 27*, 3588−3598.
34. Hung, L.-W., Wang, I. X., Nikaido, K., Liu, P.-Q., Ames, G. F.-L., and Kim, S. H. (1998) *Nature 396*, 703−707.
35. Luckacs, G. L., Mohamed, A., Kartner, N., Chang, X. B., Riordan, J. R., and Grinstein, S. (1994) *EMBO J. 13*, 6076−6086.

BI9903603